

Impact of Ionic Species on the Performance of Pedot:PSS-Based Organic Electrochemical Transistors

Renan Colucci,* Bianca de Andrade Feitosa, and Gregório Couto Faria*

The organic electrochemical transistor (OECT) has received considerable interest in the field of bioelectronics due to its ability to support both ionic and electronic transport. However, the fundamental aspects of the OECT's operation are not yet fully understood. Here, the impact on the performance of poly(3,4-ethylenedioxythiophene):polystyrene sulfonate (PEDOT:PSS)-based OECTs, of a series electrolytes with chloride-based ions is evaluated, varying their cation counterpart under the extension of the Hofmeister Series. Electrical results are analyzed using the Bernards-Malliaras and Faria-Duong models and correlated with quartz crystal microbalance measurements. It is shown that cations with a higher ability of salting-in, according to the Hofmeister series, swell the channel with higher efficiency. In addition, cations with a higher ability to salt-out promote smaller modulations in the channel's current, indicating that the ionic transport in the bulk of the channel is directly correlated with the swelling ability of the film. Overall, the results provide a better understanding of the interplay of channel and electrolyte in OECTs and promote guidelines for optimizing materials choice for highly sensitive OECTs.

1. Introduction

Organic mixed conductors (OMCs) are soft, biocompatible, and printable materials able to support both ionic and electronic transport.^[1–3] These characteristics make them selectable for a high range of applications in the bioelectronics field, such as neuromorphic devices,^[4–6] ion pumps,^[7] biosensors and bio-signal


sensors,^[8–11] etc.^[12,13] The device used in most of these applications is the organic electrochemical transistor (OECT), which has the ability to convert (and amplify) ionic fluxes into electronic flux.^[14,15] In a typical OECT, a channel composed of an OMC layer is defined between two contacts, named source and drain. The channel is in contact with an electrolyte, where a third electrode (gate) is immersed. In ideal conditions,^[16] a gate potential promotes the movement of ions from the electrolyte into the channel bulk, which are compensated by electronic charges injected by the drain. This process results in a doping/dedoping of the channel, depending on the initial state of the OMC, and therefore in a change in the electrical conductivity of the device.^[14] The basic electrical characterization of OECTs takes into account the output and transfer curves/characteristics for

steady-state behavior, and impedance spectroscopy and/or pulsed gate voltage for transient responses, similar to the electrical characterization of traditional transistors.

Complementary to the electrical characterization, theoretical models to predict the output curves are key to describe the device's working mechanisms. Indeed, one of the most used model to describe the steady-state behavior of OECTs is the Bernard & Malliaras model (B&M).^[17] The B&M model split the device into two circuits, electronic and ionic. The first one is restricted to the in-plane movement of charges and is described by a 1D Ohm law. The second one represents the off-plane movement of the ions from the electrolyte into the channel and is described by an equivalent RC circuit. Both circuits are coupled through the electronic charge carrier density, since it is dependent on the number of ions that penetrate the channel. Such a value is given by the electrical capacitance of the ionic circuit. The final equation for depletion mode OECTs is presented in the experimental section (Equation 1), and a thorough derivation is presented step-by-step in the revision article by Colucci et al.^[18] Equation 1 depends basically on two terms: the pinch-off voltage (V_p) and the product of electronic mobility and volumetric capacitance (μC^*). Both terms can be obtained by fitting the output curves using Equation 1. In the B&M model, the pinch-off voltage is mathematically defined as $(q\rho)/C^*$ and represents the voltage where the channel is fully depleted. Here, q is the elementary charge and ρ is the initial charge density of carriers in the polymer.^[19,20] The second

R. Colucci, B. de A. Feitosa, G. C. Faria
Instituto de Física de São Carlos (USP)
São Carlos 13566–590, Brazil
E-mail: rcolucci@usp.br; gcfaria@ifsc.usp.br

R. Colucci
Department of Molecular Electronics
Max Planck Institute for Polymer Research
Ackermannweg 10, 55128 Mainz, Germany
B. de A. Feitosa
Departamento de Engenharia de Materiais
Escola de Engenharia de São Carlos (USP)
São Carlos 13563-120, Brazil

 The ORCID identification number(s) for the author(s) of this article can be found under <https://doi.org/10.1002/aelm.202300235>

© 2023 The Authors. Advanced Electronic Materials published by Wiley-VCH GmbH. This is an open access article under the terms of the Creative Commons Attribution License, which permits use, distribution and reproduction in any medium, provided the original work is properly cited.

DOI: 10.1002/aelm.202300235

parameter (μC^*) is considered the benching mark of OECTs,^[21] since it correlates the electronic transport (μ) and the ability of channel's material to accumulate ionic charges (C^*). A strategy to decouple the ionic and electronic responses is efficiently achieved by measuring and fitting the drain and/or gate transient responses. Here, the Faria and Duong (F&D) model allows extracting the device's capacitance (C), by associating the ionic circuit to an equivalent R//RC loop. Equation 3, in the Experimental Section, presents the gate current as a function of time calculated by the F&D model, which is used to fit experimental data.^[22]

Recent studies have shown that the aforementioned parameters strongly depend on the characteristics and interaction between the channel materials and electrolyte composition.^[23–27] In fact, one of the requirements defined by Duong et al. to have an OECT is to ensure that the solvent is able to efficiently swell the polymer film, which has a direct impact on the volumetric capacitance.^[16] Indeed, Flagg et al. showed that the polythiophene derivative with hydrophilic ethylene glycol-based (EG) side chains poly(3-[(2-(2-methoxyethoxy)ethoxy)methyl]thiophene-2,5-diyl) (P3MEEMT) result in an OECT with higher performance when compared to the standard poly(3-hexylthiophene-2,5-diyl) (P3HT).^[23] That is because the hydrophilic side chains promote the channel swelling when in contact with aqueous electrolytes, facilitating ionic uptake by the channel. Similar results were obtained by Savva et al. studying OECTs with channels composed by dialkoxymethylthiophene-co-thienothiophene (2T-TT) with EG structures attached as side chains.^[24] In this study the amount of EG anchored to the 2T-TT molecule was varied, generating greater film swelling with increasing amount of anchored EG. As for different electrolyte compositions, Flagg et al., Cendra et al. and Samuel et al. have demonstrated that, in accumulation-mode OECTs, electrolytes composed of small ions with higher hydration spheres tend to promote higher swelling.^[25,26,28] Despite this, even with superior swelling, these electrolytes result in devices with lower performance and sensitivity. These results, at first glance, may seem contrary to the approach to increase the hydrophilicity of the polymer backbone and, therefore, counterintuitive, since greater hydration of the film should facilitate the ionic penetration and hence increase the volumetric capacitance. However, in all cited cases, the polymer's backbone is hydrophobic, which means that ions with smaller hydration sphere are easily uptake by the polymer's backbone and interact with it electrochemically more efficiently.^[24]

Although the aforementioned manuscripts have shown a clear influence of the interaction of the electrolyte-polymer, and ion-polymer on the OECT performance, they only focused on accumulation-mode OECTs based in hydrophobic materials. Since, depletion-mode poly(3,4-ethylenedioxythiophene):polystyrene sulfonate (PEDOT:PSS)-based OECTs are one of the most commonly used switching device in the bioelectronics field,^[10,29–33] it is also essential to evaluate similar phenomena in it. Indeed, the volumetric capacitance in PEDOT:PSS films is originated from the interaction between the hydrophilic sulfonate groups in PSS and the cations from the electrolyte.^[34,35] Such interaction leads to the formation of a double-layer capacitors, where each pair of cation-sulfonate acts as an individual capacitor. The distance between the two “plates” will be determined by the ionic hy-

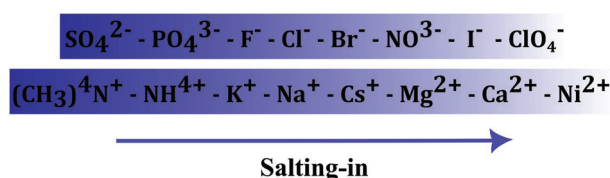


Figure 1. Schematic representation of the Hofmeister Series according to the salting-in ability of each ion. Based on references.^[42–44]

dration sphere. The overall capacitance of the PEDOT:PSS film is, therefore, the summation of those individuals capacitors. It is worth mentioning that given the PEDOT:PSS structure is formed by a two-phase morphology, being the PEDOT-rich phase the hole-conducting portion, and the PSS-rich the ion-uptaken portion, the ion-PEDOT interaction frequently happens in the interface between these two regions.^[35,36] Currently, there have been only a few studies correlating the performance of PEDOT:PSS-based OECT with the electrolyte composition. For instance, Coppede et al. developed a drift-diffusion version of the B&M model, through which they could determine the cationic species present on the electrolyte, by modeling experimental data obtained for several electrolytes. However, the model only considers the ions in the electrolyte, not counting those that penetrate into the film.^[37] Pecqueur et al. showed from transient measurements, (square pulsed voltage on the gate and constant voltage on the drain), that the drain current modulation in PEDOT:PSS-based OECTs in low frequency is higher for smaller cations and in high frequency is higher for bivalent cations.^[27] Lastly, Tsen et al. showed that it is possible to determine the composition of unknown solutions, through a two-step analysis using data from electrical impedance spectroscopy and steady-state transistor measurements. The protocol consists of a construction of an experimental calibration curve, which correlates the V_{off} and diffusion resistance (R_w^*) as a function of electrolyte concentration.^[38] The three articles abovementioned demonstrate that the change in the ionic species of the electrolyte alters the electrical responses of the PEDOT:PSS-based OECTs. However, they did not study how these changes are correlated with the physical and chemical properties of the ionic species and with the ion-polymer interaction.

The interaction between ions and macromolecules, which includes polymers, has been described by the so-called Hofmeister Series (HS).^[39] In 1888, Franz Hofmeister observed that different salts could increase or decrease the solubility of proteins in aqueous media.^[40] From empirical results, he suggested a series that classifies the ions in order of their salting-in ability (increasing of solubility), as depicted in **Figure 1**. The initial hypothesis proposed by Hofmeister to explain the results was based on a competition between dissolved salt and protein for water hydration. From that he classified the ions as kosmotropes (water makers), which in general are highly-hydrate ions and have the ability to precipitate proteins (salting-out); and chaotropes (water breakers), which are less hydrated and tend to better solubilize proteins (salting-in).^[40] Currently, new investigations suggest that direct ion-macromolecule interactions or even the properties of the ions themselves are responsible for most aspects of this phenomenon and that the initial hypothesis does not fully describe the empirical results,^[41–44] but most of the details

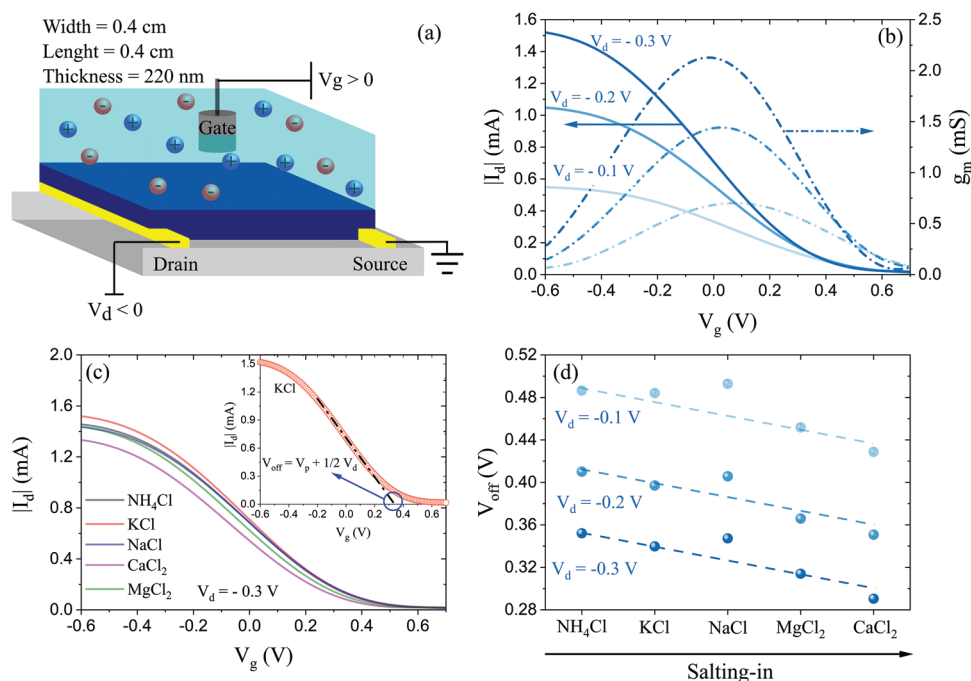


Figure 2. a) Sketch of a typical organic electrochemical transistor (OECT), depicting the transistor channel, source (S), drain (D), electrolyte, and gate (G). b) Transfer curve for an OECT with the geometry of $W = 0.4$ cm, $L = 0.4$ cm, and thickness of (220 ± 10) nm, operating with KCl based electrolyte. c) Transfer curves ($V_d = -0.3$ V) with five different electrolytes with a concentration of 100 mM. Inset: Definition of the V_{off} : the linear region of the transfer curve was extrapolated to $I_d = 0$ to extract the V_{off} . d) Plot of V_{off} for the five different salts. The error bar is lower than the radius of the dots. The x-axis is ordered following the HS. The dashed lines are visual aid to check the dependence between the V_{off} and the salting-in ability of the cationic species.

behind the origin of the HS are still unknown. Here, we carry out a thorough study on the impact of different cationic species in the performance of PEDOT:PSS-based OECTs and interpreted the results in the light of the Hofmeister Series. We have used aqueous electrolytes, keeping the chloride molecule as the fixed anion, varying the cations counterpart, in order to explore the full extension of the HS. The B&M and F&D models were used to analyze the steady state and transient electrical characteristics of the devices. To correlate the electrical parameters with the swelling of the films, electrical quartz crystal microbalance (EQCM) measurements were performed.

2. Results and Discussion

A typical OECT consists of two planar electrodes, the source and drain, connected through a semiconducting polymer, defining the transistor channel. The active layer is then placed in contact with an electrolyte, where a third electrode (gate) is immersed (see Figure 2a). Here gold-based source and drain electrodes were deposited and standard Ag/AgCl pallets were used as gate electrodes. For PEDOT:PSS-based OECT, which operates in depletion mode, positive voltages are applied to the gate electrode. Upon application of a gate voltage, cations from the electrolyte are injected into the volume of the (semi)conducting polymer. These cations compensate the sulfonated groups in the PSS chain, thereby dedoping the PEDOT, leading to a decrease of the drain current.^[2,18] The dedoping process can be easily visualized through the transfer curves, presented as solid traces in Figure 2b: a decrease of the drain current with increasing gate voltage is observed, being

consistent with the operations of depletion-mode OECTs.^[14,15] The device's ability to convert modulation in the gate voltage to changes in the drain current is given by the first derivative of the transfer curve, namely, transconductance, $g_m = dI_d/dV_g$. For the device depicted in Figure 2b, the maximum transconductance obtained was 2 mS for $V_d = -0.3$ V and $V_g = 0$ V, which is consistent with the literature.^[45]

To study the device's output dependency with different electrolytes, we have first performed transfer measurements with several 100 mM water-based electrolytes. Here, we have exploited the following salts: ammonium chloride (NH_4Cl), potassium chloride (KCl), sodium chloride (NaCl), magnesium chloride (MgCl_2), and calcium chloride (CaCl_2), comprising the entire length of the HS, (see Figure 1). As already mentioned, note that the chloride anion (Cl^-) was kept unvaried throughout the series. To guarantee no memory or cross effects between salts, we have used fresh devices, from the same fabrication batch, for each of the electrolytes. All devices herein used consist of channel dimension of 0.4 cm \times 0.4 cm ($W \times L$), with an average PEDOT:PSS thickness of (220 ± 10) nm.

Figure 2c shows the transfer characteristic of the PEDOT:PSS-based OECT for each of the exploited electrolytes. Although the overall aspect of the transfer curves are similar, their shape and current intensities are different, suggesting that the ionic motion, as well as their physical chemistry characteristics, influence the swelling properties and therefore the dedoping phenomena in OECTs. The efficiency of each cation to deplete the channel can be directly evaluated by analyzing the turn-off voltage (V_{off}) from the transfer curves. This parameter represents

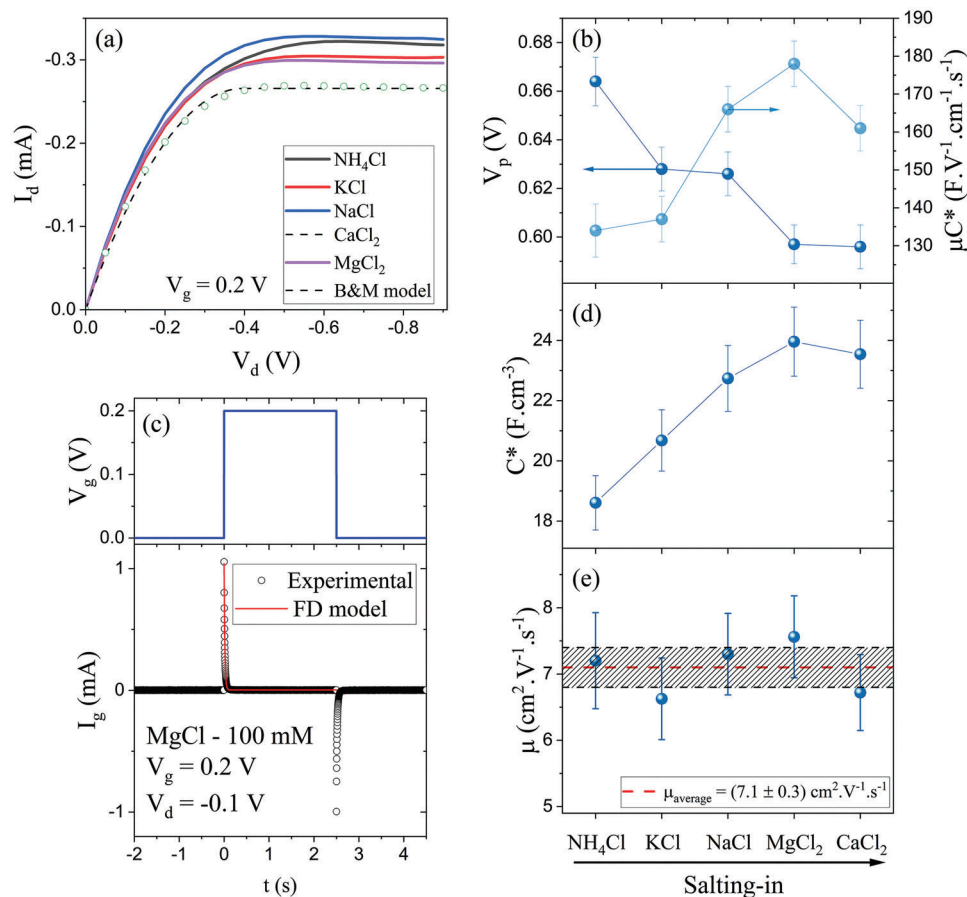


Figure 3. a) Output curves ($V_g = 0.2$ V) with five different electrolytes. Here we present the output curve from CaCl_2 (green circle) with the B&M model (black dashed line). The fitting for the other electrolytes can be found in Figure S2 (Supporting Information). b) Benchmark factor (μC^*) and V_p obtained from output curves using the B&M model for the five different salts. c) Applied gate voltage during the transient measurement (upper) and the collected gate current fitted from MgCl_2 (black circles) with the F&D model (red line) (bottom). The fitting for the other electrolytes can be found on Figure S4 (Supporting Information). d) Volumetric capacitance (C^*) obtained from transient gate curves using the F&D model for the five different salts. e) Electronic mobility calculated through the ratio ($\mu C^*/C^*$) for five different salts. All the measured parameter can be checked on the Table S1 (Supporting Information).

the gate voltage strength required to turn off the channel's current. Extrapolating the linear region of the transfer curve to $I_d = 0$, (see Inset in Figure 2c), we were able to extract the V_{off} of each of the curves, (for further details, refer to the materials and methods section). Figure 2d presents the dependency of V_{off} with the salt cations, for different drain voltages. Indeed, the V_{off} has a clear dependence with the cationic species, decreasing while the salting-in ability increases. In summary, Figure 2d suggests that cations that have a greater ability to salting-in according to HS, depletes the PEDOT:PSS film in a more efficient way. It is worth mentioning that the Na^+ cation, however, is slightly off in the trend shown in Figure 2d. We attribute this result to a possible Na^+ residues in the PEDOT:PSS, due to the synthesis process. Indeed, the monomer EDOT is polymerized in the presence of an oxidant agent (persulfate group S_2O_8). Usually, the synthetic routes make use of sodium persulfate ($\text{Na}_2\text{S}_2\text{O}_8$),^[46] which leaves behind cations of Na^+ in the final PEDOT:PSS ink, even after the dialysis step (see Figure S1, Supporting Information). Such residues seem to impact the output characteristics of PEDOT:PSS-based OECTs and lead to a slightly up-

ward shift in the V_{off} trend, when operated having NaCl -based electrolytes.

Figure 3a presents the output curves obtained for the five electrolytes, keeping $V_g = +0.2$ V. The saturation drain current clearly depends on the ionic species present in the electrolyte. Here, CaCl_2 has the smaller saturation current, while the NaCl presents the highest one. Note that, as PEDOT:PSS-based OECT operates in depletion mode, having the smallest saturation curve for a given gate voltage, means that it has the best turn-off performance within the series, i.e., CaCl_2 seems to de-dope the PEDOT:PSS film more efficiently. In addition, OECTs operated with cations in the left side of the HS, tend to achieve saturation currents at higher drain voltage, confirming that CaCl_2 , for instance, depletes the channel more effectively. This is confirmed by Figure 3b, where the fitting parameters of the B&M model of each of the output curves of Figure 3a are presented. The first parameter to be analyzed is the pinch-off voltage. Note that MgCl_2 and CaCl_2 have similar V_p , ≈ 0.60 V, with an increase to 0.66 V for NH_4Cl . This result corroborates the visual analysis of Figure 3a, confirming that the CaCl_2 depletes the channel more efficiently.

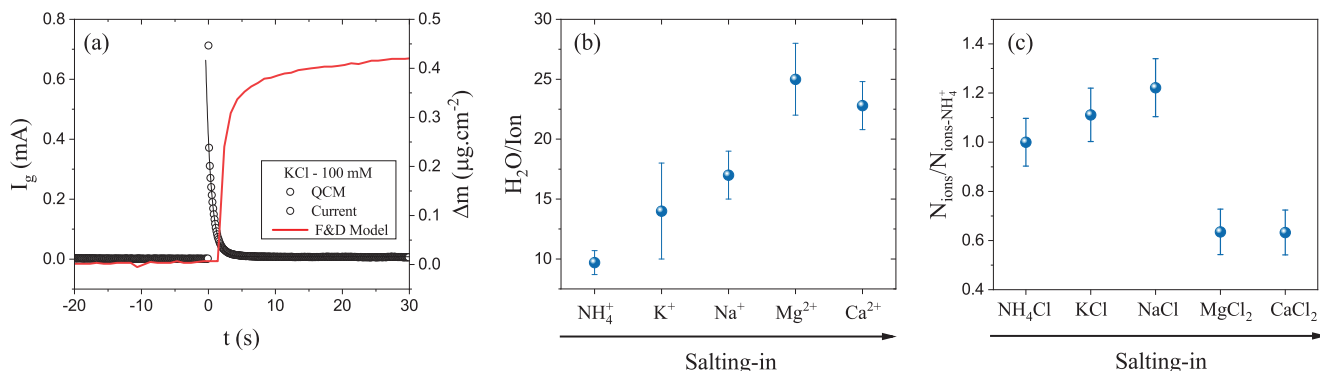


Figure 4. a) Applied gate voltage during the EQCM measurements (upper) and the collected electrical current (black dots) and change of mass density (red line) (bottom). The current and the mass density variation were measured simultaneously. The dashed blue line is the obtained fitting using the F&D model. b) Number of water molecules per cation that enter into the bulk of the PEDOT:PSS film during the dedope process for the five electrolytes studied. The error was calculated from the deviation of up to 3 measurements. c) Number of ions that penetrate in the channel bulk normalized using the NH_4^+ as reference. The values were calculated using the capacitance from Figure 4b and considering that monovalent cations have a charge equal to q and bivalent cations equal to $2q$.

On the other hand, the NH_4Cl has one of the worst output characteristics, reflected by the higher V_p number. Given that V_{off} (presented in Figure 2d) and V_p are correlated by Equation 2, it is obvious that they have similar trends and both represent a measure of the voltage strength needed to dedoping the organic semiconductor.^[47]

The B&M model allows to extract the product μC^* . Such a factor is a benching mark for evaluating OECTs performance, since it correlates two important parameters: the volumetric capacitance (C^*), which is related to ion accumulation in the channel, and the electronic mobility (μ), representing the performance of the electronic response.^[21] From Figure 3b we can observe that μC^* increases with the cations' ability to salting-in the polymer, following the HS and corroborating previously discussed results. The benching mark μC^* starts at roughly $130 \text{ F V}^{-1} \text{ cm}^{-1} \text{ s}^{-1}$ for NH_4Cl , increasing to a maximum of $180 \text{ F V}^{-1} \text{ cm}^{-1} \text{ s}^{-1}$ for $MgCl_2$, finishing $\approx 160 \text{ F V}^{-1} \text{ cm}^{-1} \text{ s}^{-1}$ for $CaCl_2$.

In Figure 3c,d, we make use of transient measurements to decouple the ionic response, given by the volumetric capacitance. Here we applied a square pulse voltage on the gate, a constant drain voltage ($V_d = -0.1 \text{ V}$) and monitor both gate and drain transient current. Figure 3c presents the gate voltage and the gate current for OECTs operated with $MgCl_2$ based electrolyte. The drain and gate current for the five studied electrolytes are presented in Figure S3 (Supporting Information). The difference between the on and off currents in Figure S3a (Supporting Information) has similar trends as observed in the output curves in Figure 2a. Figure S3b (Supporting Information), which depicts the gate transient current, suggests that each electrolyte results in a specific charging time. According to the F&D model, this is due to differences in electrolyte resistance and film capacitance, promoted for the electrolyte nature. Fitting the curves using the F&D model (Figure 3c; Figure S4, Supporting Information), we were able to extract the capacitance for each of the salt, and through the device geometry, we calculated the volumetric capacitance (shown in Figure 3d; Figure S5, Supporting Information). The volumetric capacitance increased from 18.5 F cm^{-3} for NH_4Cl up to 24 F cm^{-3} for $MgCl_2$. The trend obtained from transient measurements follows the salting-in tendencies of the

HS and is consistent with results obtained from steady-state measurements.

Once we have the benching mark factor and the volumetric capacitance, we can calculate the electronic mobility. Figure 3e summarizes the calculated results, where the electronic mobility presents an average value of $(7.1 \pm 0.3) \text{ cm}^2 \text{ V}^{-1} \text{ S}^{-1}$, which is in the same order as that already reported in the literature.^[48–50] Interestingly, the electronic mobility, in the system here explored, does not show any dependence on the ionic specie used in the electrolyte.

Finally, the OECT response was correlated to the polymer film swelling by the electrolyte,^[16,24,51] which was evaluated by electrical quartz crystal microbalance (EQCM) measurements. Figure 4a presents the electrical current and the density of mass variation response for a film dedoped with the KCl-based electrolyte (measured simultaneously). By fitting the drain-transient current with the F&D model we were able to extract the number of charges that entered into the channel's bulk. Using the mass value of the cationic species, (Table S2, Supporting Information), and their respective valence number, we were able to calculate the mass variation due to the penetration of cations into the polymer film. For all cases the mass of cations injected is smaller than the mass measured, confirming that along with the cation's species, there is a water absorption process. Since for electrolytes with low concentration ($< 1 \text{ M}$) we can assume that only cations penetrate the polymer film,^[52] then the measured surplus mass can be associated with water molecules. Using this assumption, we have built the graph presented in Figure 4b, which shows the number of water molecules per cation that enter the film. Results show that the number of water molecules per cation increases in the same order as the volumetric capacitance/merit factor (See Figure 3b,d). Since the ionic transport on PEDOT:PSS film occurs in the absorbed water,^[36] electrolytes that promote higher swelling properties allow ions to reach more crystalline regions in the polymer channel, increasing the volumetric capacitance/benching mark factor (and, of course, the dedoping process).

The flow of solvent molecules of an electrolyte through a semipermeable barrier is usually described by osmotic

pressure or correlated with the coordination number and hydration radius.^[24–26,52,53] Osmotic pressure arises due to the difference in salt concentration between the two media separated by a semipermeable membrane; in the case addressed here, the electrolyte and the semiconductor layer.^[52] Therefore, to increase the number of solvent molecules inside the channel of the OECT, the number of cations within the film must also increase. Indeed, for monovalent cations (NH_4^+ , K^+ , Na^+), the osmotic pressure can explain the results discussed in this manuscript, as seen in Figure 4c. However, this assumption fails for bivalent cations. For example, Mg^{2+} exhibits a capacitance 28% greater than NH_4^+ . However, the number of Mg^{2+} cations interacting with the PSS chains is 40% lower than the value found for NH_4^+ ions (Figure 4c). The coordination number, presented in Table S2 (Supporting Information), is a parameter that quantifies the number of water molecules distributed in the first hydration sphere of the ion. The cations used in this study have comparable coordination numbers, even so they carry different amounts of water molecules into the film. On the other hand, the hydration radius of these cations, also presented in Table S2 (Supporting Information), shows a direct relationship with the quantity of water molecules per ion that each species carries into the channel. In other words, cations with a larger hydration radius and higher valence carry more water molecules per ion, as shown by EQCM measurements (see Figure 4b). Indeed, the hydration radius is related to the ability of cations to electrostatically interact with the water molecules around them. Since cations with smaller ionic radii and higher valence establish a stronger Coulombic interaction, they are capable of interacting and holding a greater number of solvent molecules.^[54,55] However, it is important to note that the number of water molecules involved in the hydration radius should not be significantly different from the coordination number (as they are correlated). Therefore, these parameters, along with osmotic pressure, are not sufficient to individually describe our results. Thus, our findings indicate that polymer swelling by ionic species cannot be reduced to a single phenomenon or specific parameter. It is a complex interaction between the ions and the polymer macromolecule, encompassing all the physicochemical characteristics of these elements (ionic radius, hydration sphere, coordination number, valence, polymer hydrophobicity and etc). In fact, the origin of the HS considers all these properties acting together and can explain the trend of the discussed data; cations with a higher salting-in ability promote greater swelling and volumetric capacitance. Finally, based on our results, a perfect cation for obtaining an OECT with a PEDOT:PSS channel with high sensitivity should possess: 1) the smallest ionic radius; 2) the largest hydration radius, and 3) the highest valence.

3. Conclusion

We have performed a study of the impact of different cationic species on the electrical behavior of depletion-mode PEDOT:PSS-based OECTs using aqueous electrolytes. The results were correlated with the swelling of the channel's device, using the salting-in ability classification from the Hofmeister Series (HS) as reference. From transfer and output curves we demonstrated that the voltage to completely deplete the channel is directly dependent on the choice of electrolyte. Cations with greater

salting-in ability deplete the channel more efficiently, requiring then a lower V_{off}/V_p . This dependency was also reflected in the benching mark factor (μC^*), which increases with the salting-in ability of the cation. Fitting the transient gate current using the Faria-Duong model we determined that the volumetric capacitance of the channel also increases with the salting-in ability of the cationic species. Decoupling the benching mark factor, we checked that, inside of the variation range of the charge density of our results, the mobility is independent of the electrolyte. Lastly, we performed EQCM measurements to evaluate the swelling of the film and correlate it with the electrical results. Cations with greater salting-in ability were able to swell the polymer more efficiently, following the HS principle. Being so, we conclude that the dependence between the performance of the PEDOT:PSS-based OECTs and the cationic species results from the specific salting-in ability of each cation. Indeed, a greater swelling of the film facilitates the ionic diffusion into the channel's bulk and allows more crystalline regions to be accessed. Therefore, a lower V_{off}/V_p is required, and a higher volumetric capacitance is achieved. Understanding how ion characteristics change the electrical response of OECTs is one of the first steps to propose ion discrimination in biological fluids and unravel how the biological systems work. Besides that, this knowledge is indispensable to propose new materials for the active layer.

4. Experimental Section

Device Fabrication: OECTs were fabricated on wafer substrates using UV photolithography process, following a previously published protocol.^[16,56,57] Briefly, metal contacts were patterned with SPR3612, exposed with an Heidelberg MLA 150 aligner, and developed in MF-26 followed by electron beam evaporation of Ti/Au (5/50 nm respectively). Metal liftoff was done in acetone followed by a rinse with acetone/isopropanol. Two 1.5 μm thick layers of Parylene C were deposited with an SCS Labcoater 2 system, with a treatment of 3-(trimethoxysilyl)propyl methacrylate to promote adhesion of the first layer, and a diluted soap solution to prevent adhesion of the second layer. A thin (75 nm) layer of Ti was evaporated as a hard mask and patterned lithographically using the same process as above. The entire substrate was subsequently etched using a PlasmaTherm Versaline LL-ICP to define the channel dimensions. Substrates were then cleaned by ultrasonic bath in isopropanol for 5 min, followed by exposure to UV light for 5 min. Then, a dispersion of PEDOT:PSS (Clevios PH1000 from Heraeus), with 5%-vol of ethylene glycol, 0.1%-vol of dodecyl benzene sulfonic acid, and 1%-vol of 3-glycidioxypropyltrimethoxysilane was spin-coated at 1500 rpm for 60 s onto the cleaned substrates. The devices were baked at 120 °C for 1 min to peel off the parylene layer and define the geometry of channels. Then the films were baked at 120 °C for 20 min for solvent evaporation. Finally, the devices were immersed in deionized water for 24 h to remove the excess of PSS and residues from the syntheses. The geometry of the devices was $W \times L$ of 0.4 cm \times 0.4 cm and an average thickness of (220 ± 10) nm. The thicknesses were determined using profilometry Veeco Dektak 150.

Electrical Measurements: All measurements were performed using an Ag/AgCl pellets (Warner Instruments) as gate electrode. Aqueous electrolytes with five different chloride salts with concentration of 100 mM were used, namely: ammonium chloride (NH_4Cl), potassium chloride (KCl), sodium chloride (NaCl), calcium chloride (CaCl_2), and magnesium chloride (MgCl_2). Each salt had a dedicated OECT, removing any possibility of memory or cross effects on the device. The steady-state characterization was performed by the Semiconductor Characterization System Keithley 4200-SCS and the transient measurements were collected using a dual SourceMeter Keithley 2636B with a customized Python code. All the devices were submitted to a preconditioning cycle, which consists of applying a sequence of square voltage pulses at the gate from $V_g = 0.1$ to 0.5 V

(0.1 V step) using a constant $V_d = -0.05$ V. The cycle was applied 6 times, after the fourth cycle the device reached a reproducible state as can be checked in Figure S6 (Supporting Information).

The output curves were modelled using the Bernards & Malliaras (BM) model.^[18] The expression used to fit the output data is the following:

$$I_d = \frac{WD}{L} \mu C^* \left(V_p - V_G + \frac{1}{2} V_d \right) V_d \quad (1)$$

Making Equation 1 equal to zero the relation between V_{off} and V_p were calculated:

$$V_{off} = V_p + \frac{1}{2} V_d \quad (2)$$

To analyze the transient gate curves, the Faria & Duong (F&D) model was used. The F&D model could predict both drain and gate current over time upon application of square voltage pulse on the gate electrode. However, here it would focus only on the gate current. The model describes the gate current by an equivalent circuit $R//RC$. Equation 3 describes the gate current on the time. Through the model it was able to determine the resistance of the electrolyte (R_s) and the resistance (R_d) and capacitance (C_d) of the channel.^[22]

$$I_g(t) = \frac{V_g}{R_d + R_s} - \frac{V_g R_d}{R_s (R_d + R_s)} e^{-\frac{R_d + R_s}{R_d R_s C_d} t} \quad (3)$$

Electrical Quartz Crystal Microbalance (EQCM): EQCM measurements were performed using 1 in. diameter gold-coated AT quartz crystal (Stanford Research Systems, 5 MHz) substrates on an SRS QCM200 instrument coupled with the K2636B. Previous EQCM studies had shown ≈ 200 nm thick conducting polymer films exhibit a negligible change in the viscoelasticity. Therefore, the frequency (Δf) shift was a direct measure of the change in mass (Δm) within the polymer layer.^[58] In this condition, the Sauerbrey equation can be used to quantify the change in mass as described in Equation 4:

$$\Delta m = -\frac{\Delta f}{56.6} \quad (4)$$

X-Ray Photoelectron Spectroscopy (XPS): The XPS measurements were performed using a ScientaOmicron ESCA+ spectrometer with a high-performance hemispheric analyzer (EA 125) with monochromatic Al $K\alpha$ ($h\nu = 1486.6$ eV) radiation as the excitation source. The operating pressure in the ultrahigh vacuum chamber (UHV) during analysis was 2×10^{-9} mbar. Energy steps of 0.5 and 0.05 eV were used for the survey and high-resolution spectra, respectively.

Supporting Information

Supporting Information is available from the Wiley Online Library or from the author.

Acknowledgements

The authors acknowledge INCT/INEO, the Fundação de Amparo à Pesquisa do Estado de São Paulo (FAPESP) Author: Please check funding information and confirm its correctness. and the National Council for Scientific and Technological Development (CNPq) for financial support through project numbers FAPESP: 2008/57706-4 and FAPESP:2018/15670-5. G.C.F. acknowledges CNPq for financial support through project numbers 3111184/2019-7 and 406767/2018-1. In addition, this study was financed in part by the Coordenação de Aperfeiçoamento de Pessoal de Nível Superior – Brasil (CAPES) – Finance Code 001. The authors thank you, Dr. Yaakov Tuchman and Prof. Dr. Alberto Salleo

from the Stanford University for providing the OECTs substrates. The authors also would like to thank Prof. Dr. Renato Vitalino Gonçalves from the Laboratory of Nanomaterials and Advanced Ceramics (NaCA – IFSC/USP) for his assistance in the XPS characterization.

Open access funding enabled and organized by Projekt DEAL.

Conflict of Interest

The authors declare no conflict of interest.

Data Availability Statement

The data that support the findings of this study are available from the corresponding author upon reasonable request.

Keywords

Hofmeister series, ionic species, OECT, organic mixed conductors, PEDOT:PSS

Received: May 25, 2023

Revised: July 7, 2023

Published online: November 15, 2023

- [1] A. Malti, J. Edberg, H. Granberg, Z. U. Khan, J. W. Andreasen, X. Liu, D. Zhao, H. Zhang, Y. Yao, J. W. Brill, I. Engquist, M. Fahlman, L. Wågberg, X. Crispin, M. Berggren, *Adv. Sci.* **2015**, *3*, 1500305.
- [2] B. D. Paulsen, K. Tybrandt, E. Stavrinidou, J. Rivnay, *Nat. Mater.* **2020**, *19*, 13.
- [3] R. Wu, M. Matta, B. D. Paulsen, J. Rivnay, *Chem. Rev.* **2022**, *122*, 4493.
- [4] M. Giordani, M. Sensi, M. Berto, M. Di Lauro, C. A. Bortolotti, H. L. Gomes, M. Zoli, F. Zerbetto, L. Fadiga, F. Biscarini, *Adv. Funct. Mater.* **2020**, *30*, 2070187.
- [5] I. Krauthausen, D. A. Koutsouras, A. Melianas, S. T. Keene, K. Lieberth, H. Ledanseeur, R. Sheelamanthula, A. Giovannitti, F. Torricelli, I. McCulloch, P. W. M. Blom, A. Salleo, Y. van de Burgt, P. Gkoupidenis, *Sci. Adv.* **2021**, *7*, ab15068.
- [6] A. Gumyusenge, A. Melianas, S. T. Keene, A. Salleo, *Annu. Rev. Mater. Res.* **2021**, *51*, 47.
- [7] D. Cherian, A. Armgarth, V. Beni, U. Linderhed, K. Tybrandt, D. Nilsson, D. T. Simon, M. Berggren, *Flexible Printed Electron.* **2019**, *4*, 022001.
- [8] M. Berto, C. Diacci, L. Theuer, M. Di Lauro, D. T. Simon, M. Berggren, F. Biscarini, V. Beni, C. A. Bortolotti, *Flexible Printed Electron.* **2018**, *3*, 024001.
- [9] J. Hu, W. Wei, S. Ke, X. Zeng, P. Lin, *Electrochim. Acta* **2019**, *307*, 100.
- [10] J. Yu, A. Yang, N. Wang, H. Ling, J. Song, X. Chen, Y. Lian, Z. Zhang, F. Yan, M. Gu, *Nanoscale* **2021**, *13*, 2868.
- [11] Y. J. Jo, J. Ok, S. Y. Kim, T. il Kim, *Adv. Mater. Technol.* **2022**, *7*, 2001273.
- [12] A. Nawaz, Q. Liu, W. L. Leong, K. E. Fairfull-Smith, P. Sonar, *Adv. Mater.* **2021**, *33*, 2101874.
- [13] J. Y. Gerasimov, D. Zhao, A. Sultana, T. Abrahamsson, S. Han, D. Bliman, D. Tu, D. T. Simon, R. Olsson, X. Crispin, M. Berggren, S. Fabiano, J. Y. Gerasimov, D. Zhao, A. Sultana, T. Abrahamsson, S. Han, D. Tu, D. T. Simon, X. Crispin, M. Berggren, S. Fabiano, D. Bliman, R. Olsson, *Adv. Electron. Mater.* **2021**, *7*, 2001126.
- [14] J. Rivnay, S. Inal, A. Salleo, R. M. Owens, M. Berggren, G. G. Malliaras, *Nat. Rev. Mater.* **2018**, *3*, 17086.
- [15] J. T. Friedlein, R. R. McLeod, J. Rivnay, *Org. Electron.* **2018**, *63*, 398.

- [16] D. T. Duong, Y. Tuchman, P. Chakthranont, P. Cavassin, R. Colucci, T. F. Jaramillo, A. Salleo, G. C. Faria, *Adv. Electron. Mater.* **2018**, *4*, 1800090.
- [17] D. A. Bernards, G. G. Malliaras, *Adv. Funct. Mater.* **2007**, *17*, 3538.
- [18] R. Colucci, H. F. D. P. Barbosa, F. Günther, P. Cavassin, G. C. Faria, *Flexible Printed Electron.* **2020**, *5*, 013001.
- [19] V. Kaphle, S. Liu, A. Al-Shadeedi, C.-M. Keum, B. Lüssem, *Adv. Mater.* **2016**, *28*, 8766.
- [20] V. Kaphle, P. R. Paudel, D. Dahal, R. K. Radha Krishnan, B. Lüssem, *Nat. Commun.* **2020**, *11*, 2515.
- [21] S. Inal, G. G. Malliaras, J. Rivnay, *Nat. Commun.* **2017**, *8*, 1767.
- [22] G. C. Faria, D. T. Duong, A. Salleo, *Org. Electron.* **2017**, *45*, 215.
- [23] L. Q. Flagg, C. G. Bischak, J. W. Onorato, R. B. Rashid, C. K. Luscombe, D. S. Ginger, *J. Am. Chem. Soc.* **2019**, *141*, 4345.
- [24] A. Savva, R. Hallani, C. Cendra, J. Surgailis, T. C. Hidalgo, S. Wustoni, R. Sheelamanthula, X. Chen, M. Kirkus, A. Giovannitti, A. Salleo, I. McCulloch, S. Inal, *Adv. Funct. Mater.* **2020**, *30*, 1907657.
- [25] L. Q. Flagg, R. Giridharagopal, J. Guo, D. S. Ginger, *Chem. Mater.* **2018**, *30*, 5380.
- [26] C. Cendra, A. Giovannitti, A. Savva, V. Venkatraman, I. McCulloch, A. Salleo, S. Inal, J. Rivnay, *Adv. Funct. Mater.* **2019**, *29*, 1807034.
- [27] S. Pecqueur, D. Guérin, D. Vuillaume, F. Alibart, *Org. Electron. Phys., Mater. Appl.* **2018**, *57*, 232.
- [28] J. J. Samuel, A. Garudapalli, C. Gangadharappa, S. R. Mahapatra, S. Patil, N. P. B. Aetukuri, *Nat. Commun.* **2022**, *13*, 7788.
- [29] M. Braendlein, T. Lonjaret, P. Leleux, J.-M. Badier, G. G. Malliaras, M. Braendlein, T. Lonjaret, P. Leleux, G. G. Malliaras, J. Badier, *Adv. Sci.* **2017**, *4*, 1600247.
- [30] K. Guo, S. Wustoni, A. Koklu, E. Díaz-Galicia, M. Moser, A. Hama, A. A. Alqahtani, A. N. Ahmad, F. S. Alhamlan, M. Shuaib, A. Pain, I. McCulloch, S. T. Arold, R. Grünberg, S. Inal, *Nat. Biomed. Eng.* **2021**, *5*, 666.
- [31] N. Saraf, E. R. Woods, M. Peppler, S. Seal, *Biosens. Bioelectron.* **2018**, *117*, 40.
- [32] S. Yamamoto, A. G. Polyavas, S. Han, G. G. Malliaras, *Adv. Electron. Mater.* **2022**, *8*, 2.
- [33] H. F. P. Barbosa, G. D. G. Higueta, F. Günther, G. C. Faria, *Adv. Electron. Mater.* **2022**, *8*, 2100864.
- [34] C. M. Proctor, J. Rivnay, G. G. Malliaras, *J. Polym. Sci., Part B: Polym. Phys.* **2016**, *54*, 1433.
- [35] A. V. Volkov, K. Wijeratne, E. Mitraka, U. Ail, D. Zhao, K. Tybrandt, J. W. Andreasen, M. Berggren, X. Crispin, I. V. Zozoulenko, *Adv. Funct. Mater.* **2017**, *27*, 1700329.
- [36] E. Stavrinidou, P. Leleux, H. Rajaona, D. Khodagholy, J. Rivnay, M. Lindau, S. Sanaur, G. G. Malliaras, *Adv. Mater.* **2013**, *25*, 4488.
- [37] N. Coppedè, M. Villani, F. Gentile, *Sci. Rep.* **2014**, *4*, 4297.
- [38] H. Tseng, M. Cucchi, A. Weissbach, K. Leo, H. Kleemann, *ACS Appl. Electron. Mater.* **2021**, *3*, 3898.
- [39] R. Umapathi, P. M. Reddy, A. Rani, P. Venkatesu, *Phys. Chem. Chem. Phys.* **2018**, *20*, 9717.
- [40] W. Kunz, J. Henle, B. W. Ninham, *Curr. Opin. Colloid Interface Sci.* **2004**, *9*, 19.
- [41] Y. Zhang, P. S. Cremer, *Curr. Opin. Chem. Biol.* **2006**, *10*, 658.
- [42] V. Mazzini, V. S. J. Craig, *Chem. Sci.* **2017**, *8*, 7052.
- [43] B. Kang, H. Tang, Z. Zhao, S. Song, *ACS Omega* **2020**, *5*, 6229.
- [44] K. P. Gregory, G. R. Elliott, H. Robertson, A. Kumar, E. J. Wanless, G. B. Webber, V. S. J. Craig, G. G. Andersson, A. J. Page, *Phys. Chem. Chem. Phys.* **2022**, *24*, 12682.
- [45] J. Rivnay, P. Leleux, M. Sessolo, D. Khodagholy, T. Herv, M. Fioocchi, G. G. Malliaras, *Adv. Mater.* **2013**, *25*, 7010.
- [46] F. Louwet, L. Groenendaal, J. Dhaen, J. Manca, J. Van Luppen, E. Verdonck, L. Leenders, *Synth. Met.* **2003**, *135–136*, 115.
- [47] S. E. Doris, A. Pierre, R. A. Street, *Adv. Mater.* **2018**, *30*, 1706757.
- [48] J. Rivnay, S. Inal, B. A. Collins, M. Sessolo, E. Stavrinidou, X. Strakosas, C. Tassone, D. M. Delongchamp, G. G. Malliaras, *Nat. Commun.* **2016**, *7*, 11287.
- [49] M. ElMahmoudy, S. Inal, A. Charrier, I. Uguz, G. G. Malliaras, S. Sanaur, *Macromol. Mater. Eng.* **2017**, *302*, 1600497.
- [50] F. Mariani, F. Conzuelo, T. Cramer, I. Gualandri, L. Possanzini, M. Tassarolo, B. Fraboni, W. Schuhmann, E. Scavetta, *Small* **2019**, *19*, 1902534.
- [51] A. Savva, C. Cendra, A. Giugni, B. Torre, J. Surgailis, D. Ohayon, A. Giovannitti, I. McCulloch, E. Di Fabrizio, A. Salleo, J. Rivnay, S. Inal, *Chem. Mater.* **2019**, *31*, 927.
- [52] L. Bay, T. Jacobsen, S. Skaarup, K. West, *J. Phys. Chem. B* **2001**, *105*, 8492.
- [53] S. Maw, E. Smela, K. Yoshida, R. B. Stein, *Synth. Met.* **2005**, *155*, 18.
- [54] J. Zhou, X. Lu, Y. Wang, J. Shi, *Fluid Phase Equilib.* **2002**, *194–197*, 257.
- [55] B. Tansel, J. Sager, T. Rector, J. Garland, R. F. Strayer, L. Levine, M. Roberts, M. Hummerick, J. Bauer, *Sep. Purif. Technol.* **2006**, *51*, 40.
- [56] D. Khodagholy, J. Rivnay, M. Sessolo, M. Gurfinkel, P. Leleux, L. H. Jimison, E. Stavrinidou, T. Herve, S. Sanaur, R. M. Owens, G. G. Malliaras, *Nat. Commun.* **2013**, *4*, 2133.
- [57] P. Cavassin, A. M. Pappa, C. Pitsalidis, H. F. P. Barbosa, R. Colucci, J. Saez, Y. Tuchman, A. Salleo, G. C. Faria, R. M. Owens, *Adv. Mater. Technol.* **2019**, *5*, 1900680.
- [58] A. Savva, S. Wustoni, S. Inal, *J. Mater. Chem. C* **2018**, *6*, 12023.